Available online at www.sciencedirect.com
SCIENCE DIRECT®
Infrared Physics & Technology xxx (2004) xxx–xxx
INFRARED PHYSICS & TECHNOLOGY
www.elsevier.com/locate/infrared

Infrared image processing and data analysis

C. Ibarra-Castanedo, D. González, M. Klein, M. Pilla, S. Vallerand, X. Maldague *

Electrical and Computing Engineering Department, Université Laval, Quebec City (Quebec) G1K 7P4, Canada

Abstract

Infrared thermography in nondestructive testing provides images (thermograms) in which zones of interest (defects) appear sometimes as subtle signatures. In this context, raw images are not often appropriate since most will be missed. In some other cases, what is needed is a quantitative analysis such as for defect detection and characterization. In this paper, presentation is made of various methods of data analysis required either at preprocessing and/or processing images. References from literature are provided for briefly discussed known methods while novelties are elaborated in more details within the text which include also experimental results.

Keywords: Infrared thermography; Data analysis; Thermogram processing; Subsurface defect; Detection; Characterization

1. Introduction

Infrared thermography in nondestructive testing (IRNDT) provides images (thermograms) in which zones of interest (defects) appear sometimes as subtle signatures due to all factors that degrade infrared (IR) images from self-emission of the IR camera to the nonuniform properties of the surface where data are collected. Moreover, with long wavelengths in IR thermal bands (2–5 and 8–12 μm) with respect to visible bands, signals in the thermal bands are intrinsically weak since liberated photonic energy W due to the oscillatory nature of particles inside matter is inversely proportional to the wavelength. In this context, raw images are not often appropriate since most will be missed. In some other cases, what is needed is a quantitative analysis such as for defect detection and characterization.

From years to years, various methods of data analysis particularly suited in IRNDT have been developed through the World. It is interesting to notice that besides traditional techniques coming from the field of "computer vision," [1] several specific methods have been developed for IRNDT. These unique techniques are sometimes based on the underlying heat-conduction physics. These methods are required either at image preprocessing and/or processing stages. In this paper, the discussion will be devoted to such a topic. We encourage readers to consult the corresponding rich literature [2–4].

2. Preprocessing

Practically speaking, it is observed that IR images are mainly degraded by the following

* Corresponding author. Tel.: +1-418-6562962; fax: +1-418-6563594/6563159.
E-mail address: maldagx@gel.ulaval.ca (X. Maldague).

1350-4495/$ - see front matter © 2004 Published by Elsevier B.V.
doi:10.1016/j.infrared.2004.03.011

effects: • vignetting due to limited aperture, • fixed pattern noise (FPN) in commonly used focal plane arrays (FPA) due to the pixel reading procedure, • presence of dead pixels in FPA matrix and • radial distortion due to the noncolinear image points with respect optical center. Depending on a particular situation either or all of these effects have to be taken into account. Moreover nonuniform infrared and optical properties of the observed surface contribute also to the overall degradation.

Vignetting is probably the more complex effect to address since it is related to the temperature of the scene with respect to temperature of the lens with no effect present when both are identical. A correction procedure is available in [2, p. 133; 5]. FPN is cancelled out by subtracting an image of a uniform scene from the image of interest. A map of dead pixels is generally known from the FPA manufacturer. In this case the value at dead pixel locations is replaced by the average value of neighbor pixels (either four or eight neighbors are used for such purpose). A method was proposed in the literature for radial distortion correction [6]. Once these effects have been taken into account, the arbitrary thermal units g from the IR camera need to be converted into temperature [5]. The procedure consists to position the IR camera in front of a reference temperature source (such as a blackbody or a thick Copper plate) brought to various known temperatures. As the reference temperature source is varied, the IR images are recorded. Average of the central pixels in the field of view allows to get the calibration curve through a polynomial fit (example: using Matlab polyfit(...) function), in the case of our IR camera (Santa Barbara Infrared at 22.55 Hz with an integration time of 1.255 ms):

$$T\ (^{\circ}\mathrm{C}) = -25.852 + 0.0140g - 1.317 \times 10^{-5}g^2 + 7.006 \times 10^{-11}g^3 - 1.473 \times 10^{-15}g^4 \quad (1)$$

Preprocessing may include also some other procedures. Pixel enhancement is commonly used. It consists to replace a given pixel value p to a value p' depending on a nonlinear relationship $f(\ldots)$:

$$p' = f(p) \quad (2)$$

An obvious task consists to establish $f(\ldots)$ [1]. Common effects of $f(\ldots)$ includes binarization, contrast stretching with either high or low values emphasized. Since this method is pixel based, a look-up table (LUT) can be programmed for a quick processing.

Neighbor processing through a kernel is the next step. Here a kernel (of $n+1$ by $n+1$ values) is passed through the image and the central pixel value p is replaced by p' computed as follows:

$$p' = B(a_1p_1 + a_2p_2 + \ldots a_{n+1}p_{n+1}) \quad (3)$$

with B is a scaling factor, a_i are kernel weights and p_i are the $n+1$ pixel values within the kernel centered on p. Interesting effects include smoothing operator (with all weights equal to 1), high-pass filtering, Sobel operator (for edge extraction) [1].

Probably the most common preprocessing procedure is noise smoothing. Eq. (3) with all weights to unity value is popular although edges are left attenuated. Median filtering prevents this. Here to, a kernel is passed through the image and the central pixel p is replaced by the median value of the sorted kernel values. For instance if kernel has sorted values: $[21, 24, 42, 51, 83]$, p' will be set to 42. Median filtering is good to remove spiky noise. More complex noise removal techniques are available, see for instance [2, p. 196] which proposes a sliding Gaussian method. Simple subtraction techniques such as subtracting two images acquired at the same moment from two different experiments (*spatial reference technique*) or from images recorded closely (*temporal reference technique*) allow to remove unwanted effects present in both experiments such as nonuniform heating [2, p. 193]).

3. Processing

3.1. Techniques

Pulsed thermography (PT) is a common approach in IRNDT. Besides PT, lockin thermography (LT, also known as modulated thermography), step heating (SH) or vibrothermography (VT) are available. All these approaches

differ mainly by the way the specimen is thermally stimulated [2, chap. 10]. For instance in PT, an initial pulse of energy is brought to the specimen and the subsequent temperature evolution (rise and decay) is recorded while in step heating temperature is monitored during steady low power heating but for a long period of time. Although the following discussed processing techniques were originally developed for FT, they can (sometimes) be adapted to other IRNDT approaches as well.

Enhancement of the subtle signatures involves various techniques including: thermal contrast computation [2, p. 198], normalization [7], pulsed phase thermography (PPT) [2, p. 406; 8], principal component thermography (PCT) [9], 1st and 2nd derivatives [10]. Space being limited, it is not possible to discuss in details all of these techniques, interested readers are referred to cited references. Others techniques [3,4] such as, thermal tomography [2, p. 428, 11] are not discussed here.

Thermal contrast is the most common (and simpler too!). Various thermal contrast definition exist but they all share together the need to know a sound area (SoA) location within the field of view. Establishing this SoA is of course the main drawback of thermal contrast especially if automated analysis is needed or if nothing is known about the specimen. For instance absolute thermal contrast $C^a(t)$ at location of pixel p at time t is defined as:

$$C^a(t) = \Delta T(t) = T(t) - T_s(t) \tag{4}$$

with $T(t)$ is the temperature at time t at p and $T_s(t)$ is the (average) temperature at time t for the SoA.

Problem of SoA location was recently solved with the differential absolute contrast (DAC), [12]. DAC is based on Eq. (4), however instead of finding a SoA somewhere in the image, the SoA temperature at time t is computed locally at p assuming that on the first few images (at time t' in particular) local point p behaves has a SoA [12]. The mathematical development is as follows. Assuming a Dirac pulse applied to a semi-infinite body, the one-dimensional Fourier equation is solved as (z is the depth variable, $z = 0$ corresponds to the surface, Q is the injected energy at the surface, e is the thermal effusivity of the sample and ΔT is the temperature increase from $t = 0$) [2, p. 348, 13]:

$$\Delta T_{\text{semi-infinite-body}}(z = 0, t) = \frac{Q}{e\sqrt{\pi t}} \tag{5}$$

As it is well known, the solution provided by Eq. (5) diverges as time elapses and also as plate thickness enlarges with respect to the nonsemi-infinite case. Nevertheless, Eq. (5) is a good approximation.

At time t', the temperature of the sound area $Ts_{[i,j]}(t')$ is then given by:

$$\Delta Ts_{[i,j]}(t') = \Delta T_{[i,j]}(t') = \frac{Q_{[i,j]}}{e_{[i,j]}\sqrt{\pi t'}} \tag{6}$$

Assuming injected energy over the specimen is changing relatively smoothly, Eq. (6) stands and allows to extract Q/e locally:

$$\frac{Q_{[i,j]}}{e_{[i,j]}} = \sqrt{\pi t'} \cdot \Delta T_{[i,j]}(t') \tag{7}$$

From Eq. (7), the temperature of the sound area can be defined locally as a function of t:

$$\begin{aligned}\Delta Ts_{[i,j]}(t) &= \frac{Q_{[i,j]}}{e_{[i,j]}\sqrt{\pi t}} = \frac{\sqrt{\pi t'}}{\sqrt{\pi t}} \cdot \Delta T_{[i,j]}(t') \\ &= \sqrt{\frac{t'}{t}} \cdot \Delta T_{i,j}(t') \cdot (4)\end{aligned} \tag{8}$$

Finally, combining Eqs. (4) and (8) yields to the DAC formulation:

$$C^{\text{dac}}(t) = \Delta T(t) = T(t) - [t'/t]^{1/2} T(t') \tag{9}$$

Although Eq. (9) is based on a simple one-dimensional model, DAC was found particularly efficient to remove unwanted effects appearing in specimen heating for instance. Interestingly, the whole DAC procedure is now automated [14].

Normalization is a processing technique where the sum (average) of the total images to be processed is divided by the averaged set of images where the zone of interest (example a subsurface defect) is observed in the temperature data [7]. An obvious difficulty is of course to find those relevant images!

Pulsed phase thermography (PPT) goes from the time domain to the frequency domain thanks to the pixel by pixel one-dimensional discrete fast Fourier transform (FFT) of the thermal sequence:

$$F_n = \sum_{k=0}^{N-1} T(k) \mathrm{e}^{2\pi \mathrm{i} k n/N} = Re_n + \mathrm{i} Im_n \tag{10}$$

where i is the imaginary number, $T(k)$ designates the temperature at location p in the kth image of the sequence, Re and Im are respectively the real and imaginary parts of the transform and subscript n designates the frequency increment. Interestingly PPT can be seen as a link between PT and LT with several advantages since phase images ϕ_n that become available ($\phi_n = a\tan(\frac{Im_n}{Re_n})$) bring several advantages in terms of unwanted effects (optical or infrared) that cancel out somehow in the involved division. Although no SoA is involved in PPT computations, the problem to define the exact $t = 0$ was noted. Moreover, the FFT involved in the process—Eq. (10)—suppressing the direct time information makes quantitative inversion procedures tricky. This is related to the fact that Fourier transform decompose the signal of interest into infinite circular functions. For this reason, it is possible to update PPT with the Wavelet transform (WT, [2, p. 424]):

$$W_f(S,T) = \int_{-\infty}^{+\infty} f(t) h^*_{ST}(t)\, \mathrm{d}t = Re + \mathrm{i} Im\, g \tag{11}$$

where $f(t)$ is the time depending signal whose WT is computed, S is the shifting factor (associated to the frequency as in FFT) and T is the translation factor associated to the time, $f(\ldots)$ is the temporal function the Wavelet is to be computed on, t is the time, Re is the real part of the transform, $Im\, g$ is the imaginary part of the transform, i is the imaginary number ($\sqrt{-1}$), $*$ means the complex conjugate. Function $h_{ST}(t)$ is generated by translating and scaling the Mother-wavelet $h(t)$:

$$h_{S,T}(t) = \frac{1}{\sqrt{S}} h\left(\frac{t-T}{S}\right) \tag{12}$$

where S is the scaling factor that is related to the frequency and T the translation factor associated to the time. In a reported application, the Morlet-wavelet was selected as the Mother-wavelet [2, p. 424]. Since an univocal relationship exists between the translation factor and depth of zone of interest, calibration and inversion of this parameter are possible.

Principal component thermography (PCT) exploits also the decomposition of the time-varying temperature signal using "more appropriate" functions than oscillatory ones as in PPT because of the monotonic nature of IRNDT signals. In fact, PCT decomposes data into a set of orthogonal statistical modes (known as *empirical orthogonal functions* or EOF) obtained through singular value decomposition (SVD). Lets assume data are represented as a $M \times N$ matrix $\mathbf{A}$ ($M > N$). Then the SVD allows to write:

$$\mathbf{A} = \mathbf{U}\mathbf{R}\mathbf{V}^{\mathrm{T}} \tag{13}$$

with $\mathbf{R}$ being a diagonal $N \times N$ matrix (with singular values of $\mathbf{A}$ present in the diagonal), $\mathbf{U}$ is a $M \times N$ matrix, $\mathbf{V}^{\mathrm{T}}$ is the transpose of an $N \times N$ matrix (characteristic time). If IRNDT data (typically temperature are used) is arranged as time along the columns and space along the rows, then it is shown that the columns of $\mathbf{U}$ represent a set of EOFs describing spatial variations of data, the first being associated to the spatial field with exponential decay and the second to the nonuniform field correlated with structural anomalies. This second EOF is known as the PCT [9]. Interestingly, $svd(\ldots)$ function is available in Matlab although the simultaneous manipulation of three matrixes limits the size of involved matrixes. Interestingly, a theorem exists saying that every $N \times M$ matrix has a singular value decomposition.

As stated in Section 1, noise is a disturbing factor in IRNDT. Researchers thus proposed to fit the temperature decay curve in PT since it varies (in first approximation) as $t^{1/2}$ [10]. Using logarithms this yields to:

$$\ln[T(t)] = C - \frac{1}{2}\ln(\pi t) \tag{14}$$

First term in Eq. (9) corresponds to an offset related to the absorbed energy and material property and second to a straight line of slope −1/2. Next, a n-degree polynomial is fitted for each pixel p within the field of view:

$$\ln[T(t)] = a_n\{\ln[t]\}^n + a_{n-1}\{\ln[t]\}^{n-1} + \cdots + a_1 \ln[t] + a_0 \tag{15}$$

Typically, n is set to 4 or 5 to avoid "ringing" and insure a good correspondence between data and fitted values. Matlab provides a direct polynomial fitting function (polyfit(...)). Such synthetic data processing brings interesting advantages such as: significative noise reduction, possibility for analytical computations (such as the PPT), significative less storage required since the whole data set is reduced to n images (one per coefficient). This technique of temperature "reconstruction" is called thermographic signal reconstruction (TSR). In addition to raw temperatures that can be reconstructed in TSR, it was shown recently that first and particularly second time derivative were efficient at deciphering faint signals [10].

In order to illustrate (and compare) the discussed image processing techniques, a Kevlar composite panel in which artificial defects were embedded at manufacturing stage was tested. Fig. 1 shows the specimen layout while Fig. 2 illustrates

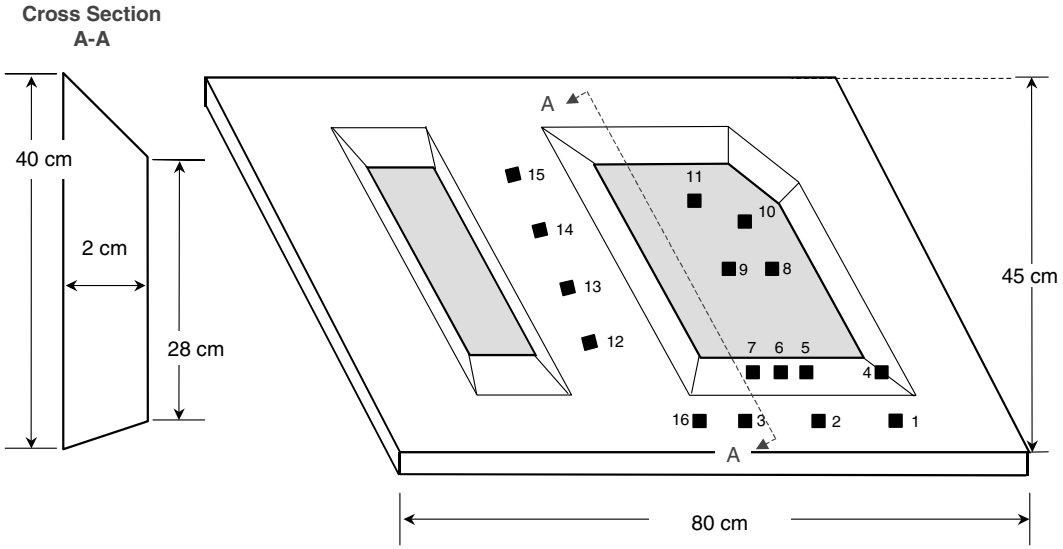

Fig. 1. Kevlar panel with nonplanar surface. Locations of 16 inclusions are shown.

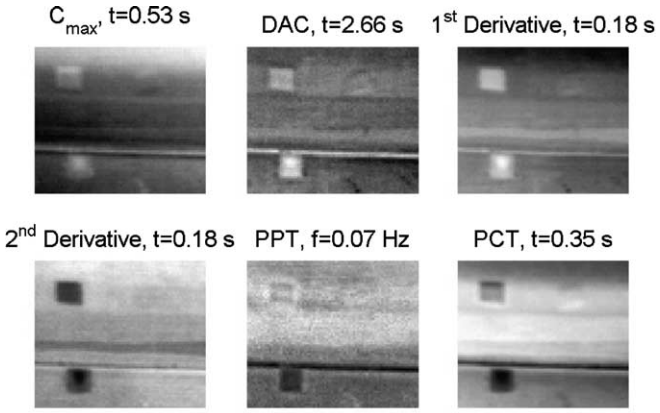

Fig. 2. Processed thermograms computations of thermal contrast, differential contrast, PPT, PCT, TSR 1st and 2nd derivatives for defects #3, #6, #7 identified in Fig. 1.

the computations of thermal contrast, differential contrast, PPT, PCT, TSR 1st and 2nd derivatives for three identified defects in Fig. 1. In summary, for the 16 present inclusions, DAC was able to resolve: 12 out of 16, TSR 2nd: 9/16, TSR 1st: 8/16, PPT: 6/16 (although better results could be expected with higher sampling rate and longer experiment duration), PCT: 6/16 and thermal contrast: 6/16. It is also noted that TSR 1st derivative and PPT generally provide images with crisper edges. Of course such "study" based on the visual perception of the viewer is quite subjective but is in line with other similar studies [7]. Moreover, depending on the application a particular technique could distinguish itself significatively so it is advised better to be cautious in regards of this observed ranking.

3.2. Quantitative processing: defect detection algorithms

This is another important step. Several approaches are possible. Manual identification by an experienced observer is the most common since the combination eye-brain is astonishingly good at quickly resolving tiny details (as in Fig. 2). On the automated side sometimes required on the plant floor in case of routine inspection, different algorithms have been proposed. Thresholding (of processed-contrast, PPT, PCT, TSR-images) is common. For instance, threshold can proceed with a fixed value (case of Eq. (2) above) or automatically by analyzing the image histogram and finding valleys where thresholding will be successful at segmenting regions of interest. In fact segmentation is a whole research field in machine vision and involves many different approaches [1].

In the particular context of IRNDT, neural networks (NNs) and ad hoc algorithms have been applied successfully [2, chap. 6]. In the particular case of NNs, contrast images are first computed and the analysis proceeds pixel by pixel with contrast values used as input to the network and with a defect/nondefect output flag. Kohonen or multilayer perceptron (MLP) were applied in this context. Interestingly, with more outputs to the network, more complex decision such as depth classification can take place.

3.3. Quantitative inversion methods

This is the ultimate data analysis step possible since a map of thermal specimen properties such as thermal diffusivity becomes available. Due to adverse conditions in IRNDT (Section 1), reported accuracies can vary greatly from a few percents to over hundred percents [2, chap. 10]! One has thus to be particularly cautious in applying these methods in each context.

Several methods have been proposed [2, chap. 10]. All rely on a sort of calibration either with a thermal model or with various specimens representative of unknown ones. For instance, one can compute defect depth z by extracting a few parameters on the thermal contrast curve such as the maximum contrast $C_{c\_\max}$ and its time of occurrence $t_{c\_\max}$ [13]:

$$z = A t_{c\_\max}^{1/2} C_{c\_\max}^{h} \tag{16}$$

with parameters A and h obtained from the calibration process. Other empirical relationships have been proposed for thermal resistance R. We already discussed in previous sections the capabilities of neural networks in term of depth sorting.

Statistical behavior of regions of interest such as background and defects have also being exploited for depth classification. The principle is that temperature, phase and amplitude can be modelled under some circumstances (such as in case of "white" noise sources) by a Gaussian random process [2, p. 417]. This statistical technique involves two phases. First a calibration or "learning phase" in which data images with defects of known depths and background location are made available so that local means m and standard deviation s are computed at each time increment and for each zone of interest (background and known defects). In the subsequent analysis step, unknown pixels are analyzed and individual probabilities are computed with m and s for a given pixel to be part of a given class. Assuming statistically independent events, individual probabilities (at different time increment) can be multiplied together to form a global probability. The winning rule is then simple: the largest wins. This statistical method was tested with raw temperature, phase and amplitude (from PPT) and re-

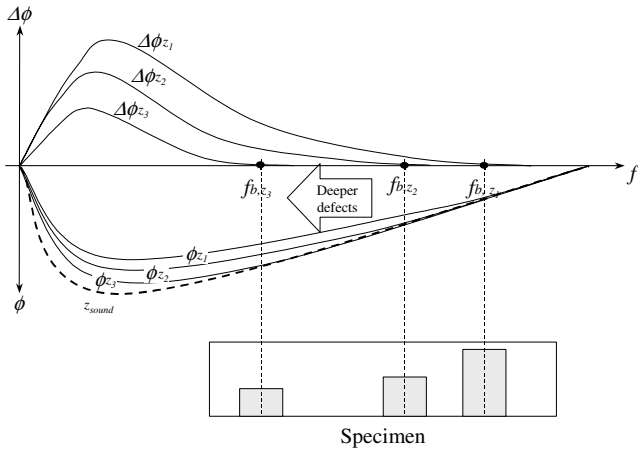

Fig. 3. Blind frequency relationship with defect depth.

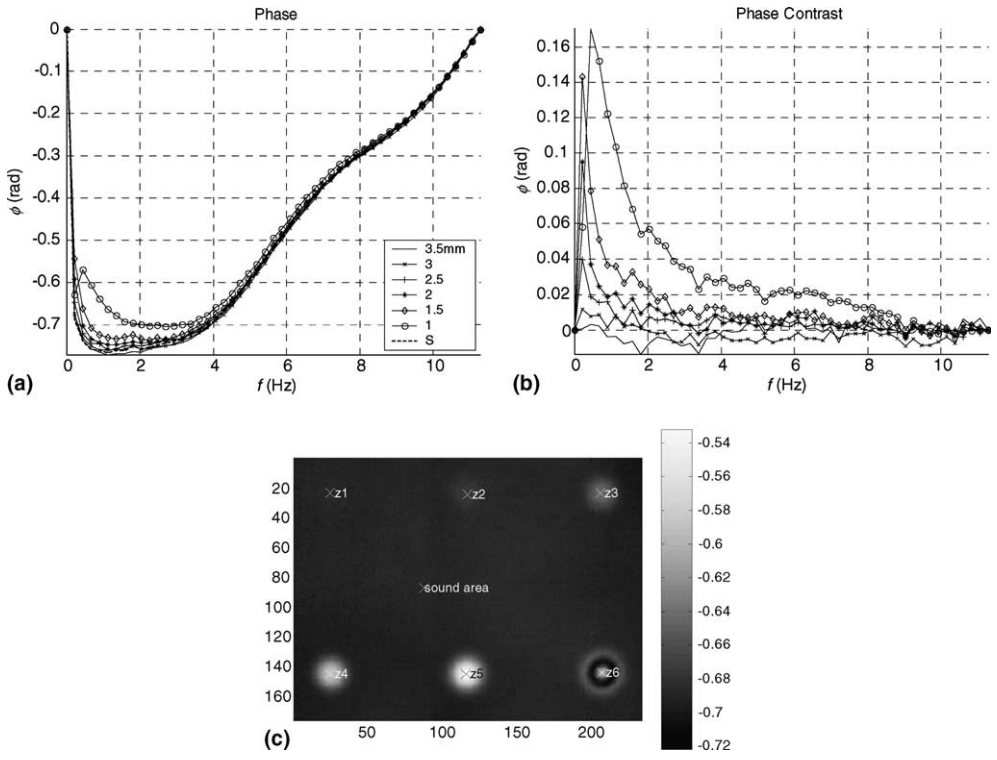

Fig. 4. Plexiglas specimen with flat-bottom holes 10 mm diameter at depth (top row, left to right): 3.5, 3, 2.5 mm and (bottom row): 2, 1.5, 1 mm. (a) Raw phase in PPT (image sampling rate: 22.55 Hz), (b) phase contrast profiles from (a). (c) Phase image at $f = 0.0188$ Hz showing defect location.

vealed quite efficient, at least on relatively simple geometries in isotropic material. This method is now adapted to more complex specimens and materials (such as anisotropic composites).

Blind frequency based on phase is a newcomer in quantitative inversion [15]. Lets remember that for a thermal wave, phase ϕ defines as $\phi = \frac{z}{\mu}$ where μ is the thermal diffusion length expressed by $\mu = \sqrt{2\alpha/\omega}$ with modulation frequency ω and, thermal diffusivity α, so that:

$$z \propto \frac{1}{\sqrt{\omega}} \tag{17}$$

As noted, with the thermal diffusion length definition, there will be modulation frequencies for which defects will not be visible. In fact (as in ultrasonics) high frequency thermal waves propagate close to the surface and inversely, low frequency thermal waves propagate deeper. By identifying the thresholding frequency called the blind frequency ω_b [15] and defined as the frequency for which a defect at a given depth becomes visible, an inversion procedure can be devised. Now lets introduced the phase contrast defined similarly to the thermal contrast in Eq. (4):

$$\Delta\phi = \phi - \phi_s \tag{18}$$

where ϕ_s is the phase value in a reference sound area (SoA). Interestingly, on $\Delta\phi(\omega)$ curves, ω_b corresponds to the point where phase reaches zero (Fig. 3). In experimental situations where noise is present, it is necessary to introduce a certain threshold (example of 0.03 rad on Fig. 4) to estimate ω_b. Next depth is extracted from the calibrated line of z versus $[1/\omega]^{1/2}$. Preliminary investigations of this approach are encouraging (as shown on Fig. 5).

Defect sizing is generally achieved by extracting the contour of the detected anomaly either at peak contrast slope, at peak maximum thermal contrast or as early as possible once the anomaly comes out of the noise to avoid the lateral thermal diffusion (that tends to enlarge the size at peak contrast or slope). An iterative technique was also proposed and consists to extract the contour in each (contrast) image at half maximum amplitude. A plot of the size as function of the square root of the time is then established and the extrapolated line at time zero yield to a good estimation of defect size [16].

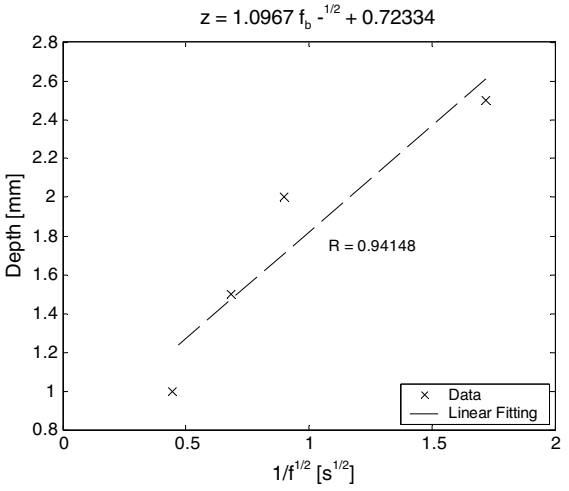

Fig. 5. Calibrated line of depth z versus $[1/\omega]^{1/2}$. Notice the two deepest defects shown in Fig. 4c did not produce a phase contrast sufficient to be taken into account in the inversion (due to the noise level and phase contrast threshold).

4. Conclusion

In this paper, various data analysis methods were presented at preprocessing and processing levels and also for defect detection and quantitative characterization in IRNDT. These methods increase IRNDT capabilities since subtle defects signature become apparent. More sensitive and fast IR cameras coupled with always more powerful computers capable to handle efficiently complex algorithms and large data set should push these limits even further. In fact, one can say that more is to come.

Acknowledgements

The support of the Natural Sciences and Engineering Research Council of Canada is acknowledged.

References

[1] W.K. Pratt, Digital Image Processing, Wiley, New York, 1991, p. 698.
[2] X. Maldague, Theory and Practice of Infrared Technology for NonDestructive Testing, John Wiley-Interscience, 2001, 684 p..

[3] Biannual Quantitative Infrared Thermography Conferences (QIRT): http://www.gel.ulaval.ca/qirt/.
[4] Annual Thermosense conferences organized by the SPIE (The International Society for Opti-cal Engineering): http://www.thermosense.org/.
[5] S. Marinetti, X. Maldague, M. Prystay, Calibration procedure for focal plane array cameras and noise equivalent material loss for quantitative thermographic NDT, Mater. Eval. 55 (3) (1997) 407–412.
[6] J. Heikkilä, O. Silvén, A four-step camera calibration procedure with implicit image correction, IEEE Trans. Pattern Anal. 22 (10) (2000) 1066–1077, see also Matlab source code at: www.vision.caltech.edu/bouguetj/calib_doc/.
[7] J.N. Zalameda, N. Rajic, W.P. Winfree, A comparison of image processing algorithms for thermal nondestructive evaluation, in: K.E. Orlando, X. Cramer, X. Maldague (Eds.), SPIE Proc. Thermosense XXV, vol. 5073, 2003, pp. 374–385.
[8] X. Maldague, S. Marinetti, Pulse phase infrared thermography, J. Appl. Phys. 79 (Mar) (1996) 2694–2698.
[9] N. Rajic, Principal component thermography for flaw contrast enhancement and flaw depth characterisation in composite structures, Compos. Struct. 58 (2002) 521–528.
[10] R.E. Martin, A.L. Gyekenyesi, S.M. Shepard, Interpreting the results of pulsed thermography data, Mater. Eval. 61 (5) (2003) 611–616.
[11] V.P. Vavilov, Dynamic Thermal Tomography: Perspective Field of Thermal NDT, in: S.A. Semanovich (Ed.), Proc SPIE Thermosense XI, vol. 1313, 1990, pp. 178–182.
[12] M. Pilla, M. Klein, X. Maldague, A. Salerno, New Absolute Contrast for Pulsed Thermography, in: D. Balageas, G.M. Busse, G. Carlomagno (Eds.), QIRT 2002, pp. 53–58.
[13] D.L. Balageas, A.A. Déom, D.M. Boscher, Characterization and nondestructive testing of carbon-epoxy composites by a pulsed photothermal method, Mater. Eval. 45 (4) (1987) 465–466.
[14] D. González, C. Ibarra-Castenado, M. Pilla, M. Klein, X. Maldague, Automated Differential Absolute Contrast, in submission process to QIRT 2004.
[15] W. Bai, B.S. Wong, Evaluation of defects in composite plates under convective environments using lock-in thermography, Meas. Sci. Technol. 12 (2001) 142–150.
[16] D.P. Almond, S.K. Lau, Defect sizing by transient thermography I. An analytical treatment, J. Phys. D Appl. Phys. 27 (5) (1994) 1063–1069.